N89-21741

1988

NASA/ASEE SUMMER FACULTY FELLOWSHIP PROGRAM

MARSHALL SPACE FLIGHT CENTER
THE UNIVERSITY OF ALABAMA

TRANSIENT NATURAL CONVECTION HEAT AND MASS TRANSFER IN CRYSTAL GROWTH

Prepared by:	Samuel S. Han
Academic Rank:	Associate Professor
University and Department:	Tennessee Technological University Mechanical Engineering
NASA/MSFC:	
Laboratory:	Structure and Dynamics
Division:	Earth Science and Applications
Branch:	Fluid Dynamics
MSFC Colleague:	Charles F. Schafer Cheryl Morroni
Date:	August 10, 1988
Contract No.:	NGT 01-002-099 The University of Alabama

TRANSIENT NATURAL CONVECTION HEAT AND MASS TRANSFER IN CRYSTAL GROWTH

by

Samuel S. Han
Associate Professor of Mechanical Engineering
Tennessee Technological University
Cookeville, Tennessee 38505

ABSTRACT

A numerical analysis of transient combined heat and mass transfer across a rectangular cavity is performed by a numerical method based on the SIMPLE algorithm. The physical parameters are selected to represent a range of possible crystal growth in solutions.

Numerical results are compared with available experimental data to confirm the accuracy of the results. Good quantitative agreements are obtained for the average mass transfer rate across the cavity. Also, qualitative agreements are observed for the global development of thermal and solute fields.

It is found that the thermal and solute fields become highly oscillatory when the thermal and solute Grashof numbers are large. Oscillations are probably caused by number of different instability mechanisms. By reducing the gravity some of these instabilities were made to disappear at the lower Grashof numbers.

Transient temperature and solute distribution near the crystal growing surface are highly non-uniform at the higher Grashof numbers. These non-uniformities are less severe in the reduced gravity environments but still exist. The effects of convection on the rate of average mass transfer are more than one order of magnitude higher than those of conduction in the range of Grashof numbers studied. Dependency of mass transfer rate on the Grashof number indicates that the convection effects may not become negligible even in the microgravity environments for the range of parameters investigated.

ACKNOWLEDGEMENT

I would like to offer my deepest gratitude to Dr. Charles F. Schafer and Ms. Cheryl Morroni, my MSFC colleagues, for giving me an opportunity to learn the importance of single crystals and to appreciate intricate transport processes involved in crystal growth.

Without help, advice and guidance from many collegues in the Fluid Dynamics Branch, my stay at Marshall could be a difficult one. Many thanks to Drs. Chen, Ramachandran, Decker and Yeshola and to Mr. Trinh and Ms. Janti.

Dr. Michael Freeman and Ms. Ernestine Cothran, Co-directors of 1988 program, deserve a special gratitute for their excellent administrative help and guidance.

I. INTRODUCTION

Single crystals are important parts of modern scientific and engineering equipments because of their unique electro-magnetic properties. Most single crystals are made by one of three methods: vapor growth, solution growth and melt growth.

The final transport process in crystal growth is the phase change from liquid to solid at the growing interface. Mass transport is dominantly controlled by the mass diffusion near the interface between the liquid and solid. Thermodynamic and transport properties near the growing surface are however intimately connected to the thermal and solute fields far away from the interface. These far-field behaviors are determined by the convective heat, mass and momentum transport processes [1].

Convective transport processes tend to expedite the mass transport of crystal materials across the ampoule. Highly non-uniform temperature and solute distributions inherent in convection, however, have undesirable effects on the quality of crystals. Convection effects, in parts , are believed to be responsible for non-uniform properties of single crystals grown in vapor and solution growth and helical segregation of impurities in crystals grown in melt growth [2,3].

To improve the quality of single crystals, quantitative assessment of convection effects are required. In recent years, many research efforts, both analytical and experimental approaches, are reported in literatures [4,5,6,7]. Since the actual processes involved in crystal growth are quite complex and some of the physical processes are not well understood, most of these investigations focused on a few limited aspects of convective processes.

The objective of the present research is to investigate the transient heat and mass transfer in a two-dimensional rectangular ampoule in a solution growth by a numerical analysis. Methods of analysis are presented in section 2, numerical results are presented and discussed in section 3, followed by conclusions and recommendations in section 4.

II. METHODS OF ANALYSIS

Description of the Problem

Actual physical mechanisms involved in crystal growth are time-dependent, three-dimensional convection-diffusion processes with a phase change at the crystal growing surface. Enthalpy of phase transformation might be involved in certain applications. In general, crystal growing surfaces are not flat and they move at the rate of growing crystals. Boundary conditions imposed on the ampoule surfaces can be quite complex. Physical properties of the mixture in the ampoule might be stronly dependent upon the solute concentration and temperature.

The present research is concerned with the prediction of solute and temperature fields encounterd in solution growth. To make the analysis feasible, number of simplifying assumptions are introduced in formulating the problem. The geometry of the ampoule is rectangule with a fixed aspect ratio. The left vertical wall is kept at a higher constant temperature and a higher concentration of crystal material while the right vertical wall is kept at a lower temperature and a lower concentration of crystal material. A binary mixture made of a nutrient crystal material and a carrier fluid fills the cavity of the ampoule. The crystal materials are dissolved from the left wall and deposited on the right wall. Horizontal surfaces are adiabatic and impermeable to both components. The vertical walls are also impermeable to the carrier fluid. Figure 1 shows the geometry of the ampoule considered in the present analysis.

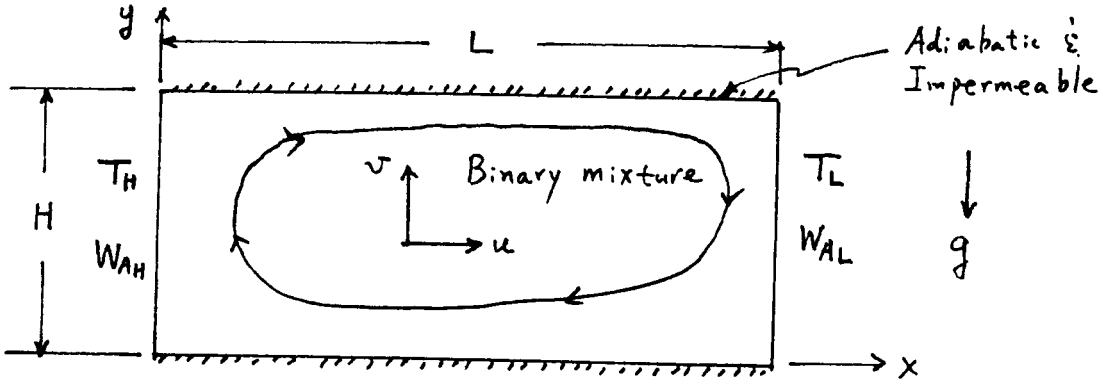

Figure 1. Geometry of the problem

Governing Equations

Assuming a two-dimensional incompressible flow of Newtonian fluid for the mixture, conservation of mass, momentum, energy and crystal material (hereafter called species A) may be expressed by the following partial differential equation:

$$\frac{\partial \rho\phi}{\partial t} + \frac{\partial}{\partial x}\left[\rho u\phi - \Gamma\frac{\partial \phi}{\partial x}\right] + \frac{\partial}{\partial y}\left[\rho v\phi - \Gamma\frac{\partial \phi}{\partial y}\right] = S \qquad (1)$$

where ϕ is the dependent variable, Γ is the diffusion coefficient and S is the source. These values are listed in Table 1 for each equations. In this expression, t is time, x and y are horizontal and vertical distance, u and v are fluid velocity in x- and y-directions, E is the internal energy, W_A is the mass fraction of species A, ρ is the density of the mixture, T is the temperature, p is the pressure, μ is the dynamic viscosity, is the thermal conductivity and D_{AB} is the mass diffusivity.

Table 1. Components of governing equations

equation	ϕ	Γ	S
mass	1	0	0
x-momentum	u	μ	$-\partial p/\partial x$
y-momentum	v	μ	$-\partial p/\partial y + \rho g \beta (T-T^\circ) + \alpha_A \rho g (W_A - W_A^\circ)$
energy	E	K/c_v	0
concentration	W_A	ρD_{AB}	0

It is assumed that the density of the fluid remains at a constant value and the effects of heat and mass transfer from the vertical walls appear as the buoyancy force along the y-direction. This is known as a Boussinesq approximation and is valid when the temperature difference between the walls are small and the mass fraction of species A is small (dilute solution). In terms of Boussinesq approximation, the density of the mixture is given by

$$\rho = \rho^\circ \left[1 - \alpha_A (W_A - W_A^\circ) - \beta (T - T^\circ) \right], \qquad (2)$$

where, β and α_A are the thermal and solute expansion coefficient, respectively. They are

$$\beta = -\frac{1}{\rho} \left(\frac{\partial \rho}{\partial T} \right)_p , \qquad (3)$$

and

$$\alpha_A = M_o (M_B - M_A) / M_A M_B , \qquad (4)$$

where

$$1/M_o = W_A^\circ / M_A + W_B^\circ / M_B , \qquad (5)$$

M_A and M_B are the molecular weight of species A and B (carrier fluid), respectively. Superscript '0' implies a reference state.

Initial and Boundary Conditions

Initially, a mixture with a constant temperature (T°) and mass fraction (W_A°) is in hydrostatic equilibrium under a given gravity (g). At t>0, temperature at the left wall is increased by a small amount and the temperature at the right wall is decreased by the same amount. Heat transfer occurs from the left wall to the adjacent fluid by conduction. Density of heated fluid, in general, becomes small and the thermal buoyancy force acts in the opposite direction to the gravity. Cooled fluid adjacent to the right wall moves in the same direction as the gravity. This buoyancy force due to the thermal effects drive the convection in the ampoule. When the concentration of species A at the left wall is increased from its initial state and decreased by the same amount at the right wall, convection occurs due to solutal buoyancy force. If $M_A > M_B$, buoyancy force due to mass transfer will act downward near the left wall and upward near the right wall. In this case, two bouyancy forces will act in the opposite direction (opposing convection). If $M_A < M_B$, then two bouyancy forces will act in the same direction (aiding convection).

Mathematically, the initial conditions are

$$u(X,Y,t=0) = v(X,Y,t=0) = 0 \quad ;$$
$$\rho(X,Y,t=0) = \rho^\circ \quad ; \quad T(X,Y,t=0) = T^\circ \qquad (6)$$
$$W_A(X,Y,t=0) = W_A^\circ .$$

and the boundary conditions are

$$T(X=0,Y) = T_H \quad ; \quad T(X=L,Y) = T_L \quad ;$$
$$W_A(X=0,Y) = W_{AH} \quad ; \quad W_A(X=L,Y) = W_{AL} \quad ;$$
$$\left.\frac{\partial T}{\partial Y}\right|_{X,Y=0} = \left.\frac{\partial T}{\partial Y}\right|_{X,Y=H} = \left.\frac{\partial W_A}{\partial Y}\right|_{X,Y=0} = \left.\frac{\partial W_A}{\partial Y}\right|_{X,Y=H} = 0 \quad ; \qquad (7)$$
$$u(X,Y=0) = v(X,Y=0) = u(X,Y=H) = v(X,Y=H) = 0 \quad ;$$
$$u(0,Y) = v(0,Y) = u(L,Y) = v(L,Y) = 0 .$$

Nondimensional Parameters

Selecting H, ν/H, ΔT and ΔW_A as the characteristic values, it can be readily shown from the governing differential equations that there are five nondimensional parameters which characterize the transport processes in the ampoule. They are

$$A = H/L \quad ; \quad P_r = \nu/\alpha \quad ; \quad S_c = \nu/D_{AB} \quad ;$$
$$G_{r_T} = g\beta\Delta T H^3/\nu^2 \quad ; \quad G_{r_S} = g\alpha_A \Delta W_A H^3/\nu^2 . \qquad (8)$$

where $\Delta T = T_H - T_L$ and $\Delta W_A = W_{AH} - W_{AL}$.

Numerical Method

The numerical method used to solve the given equations subject to the initial and boundary conditions is a modified version of the SIMPLE algorithm [8]. The SIMPLE and its many variants have been successfully applied to a wide range of fluid flow and heat transfer problems. The present method follows exactly the same procedures as described in ref.[8] except a simple modification to account for the density change due to the pressure change [9]. In solving the continuity equation, a recommendation given in ref.[10] is used to speed up the convergence.

III. RESULTS AND DISCUSSIONS

Physical Parameters

The physical size of the ampoule and the mixture properties are selected to match with some of experimental data reported in ref.[7] in terms of nondimensional parammeters. Three nondimensional parameters are fixed at constant values. They are A=0.498, Pr=7.07 and Sc=2140. Remaining two nondimensional parameters are varied to analyse the effects of their magnitude and the effects of opposing and aiding buoyancy forces. Table 2 shows these parameters for 5 cases studied in the present investigation.

Table 2. Grashof numbers (Gr_T, Gr_S) and buoyancy ratio (N)

Case	Gr_T	Gr_S	$N=Gr_S/Gr_T$
1	4.36E+5	8.12E+6	18.62
2	4.36E+5	-8.12e+6	-18.62
3	4.36E+4	8.12E+5	18.62
4	4.36E+4	-8.12E+5	-18.62
5	4.36E+3	8.12E+4	18.62

Experimental data are available for cases 1 and 2. They are used to check the accuracy of the present analysis. Smaller Grashof numbers used in cases 3-5 are obtained by reducing the gravity to 0.1 g and 0.01 g, where g=9.81 m/s^2. This approach is used to examine the effects of the reduced gravity when the mixture properties remain constant.

Numerical Parameters

Numerical results depend on the choice of numerical

parameters, such as the mesh sizes, time steps, relaxation coefficients and a convergence criterion.

The number of control volumes and their arragements are usually determined by a trial and error method until the numerical results agree with known data or become grid independent. It was reported in a previous investigation that 26 (horizontal) by 20 (vertical) control volumes gave sufficiently accurate average heat or mass transfer rate when the heat or mass transfer occurs separately [11]. A highly nonuniform grid arrangement was used in that study. The control volume sizes near the vertical walls were selected such that thin solute boundary layer developed on these surfaces contained more than one control volumes. In the same study, 26 by 20 grid system was also used for combined heat and mass transfer. Overall average mass transfer rate was seen in good agreement with experimental data. However, numerical results failed to exhibit intricate three layered convection loops observed in the experiment [1,7]. Subsequent experiments on the grid arrangement (30 by 28 and 40 by 40) reavealed that increasing grid number in the vertical direction gave improved resolution of flow structure but the average mass transfer rates were not significantly changed beyond those obtained by the 26 by 20 system. In the present analysis, a 40 by 40 grid system is used for all cases.

In the present study, numerical integration begins with a physically realistic initial condition. Consequently, convergence of numerical solutions at each time level is achieved with a few iterations provided that a proper time step is used. At the beginning of computation an extreamly small time step is used. In the subsequent computations, time steps are automatically adjusted depending on whether the number of iteration to achieve the convergence is below or above the preset minimum (2) and maximum (10) number of iterations . The convergence of flow quantities in each time step is assumed when the relative residual mass in every control volume is less than 0.1 %.

The relaxation coeffcients for the momentum equations were 0.5 for both directions and no relaxation is used for the pressure and energy equations.

Transient Global Flow Fields

Figure 2 shows transient global development of momentum, thermal and solute fields for case 1 at three different time steps. The velocity vector (top panel) and stream function (second from top) distribution show the effects of mass transfer on the convection. Since the thermal diffusivity is much larger than the mass diffusivity (Sc/Pr = 300), the convection loop in the ampoule is determined by the thermal effects only at the beginning stage of convection. However, the presence of mass transfer soon begins to modify the thermally driven convection through the double diffusive effects [12].

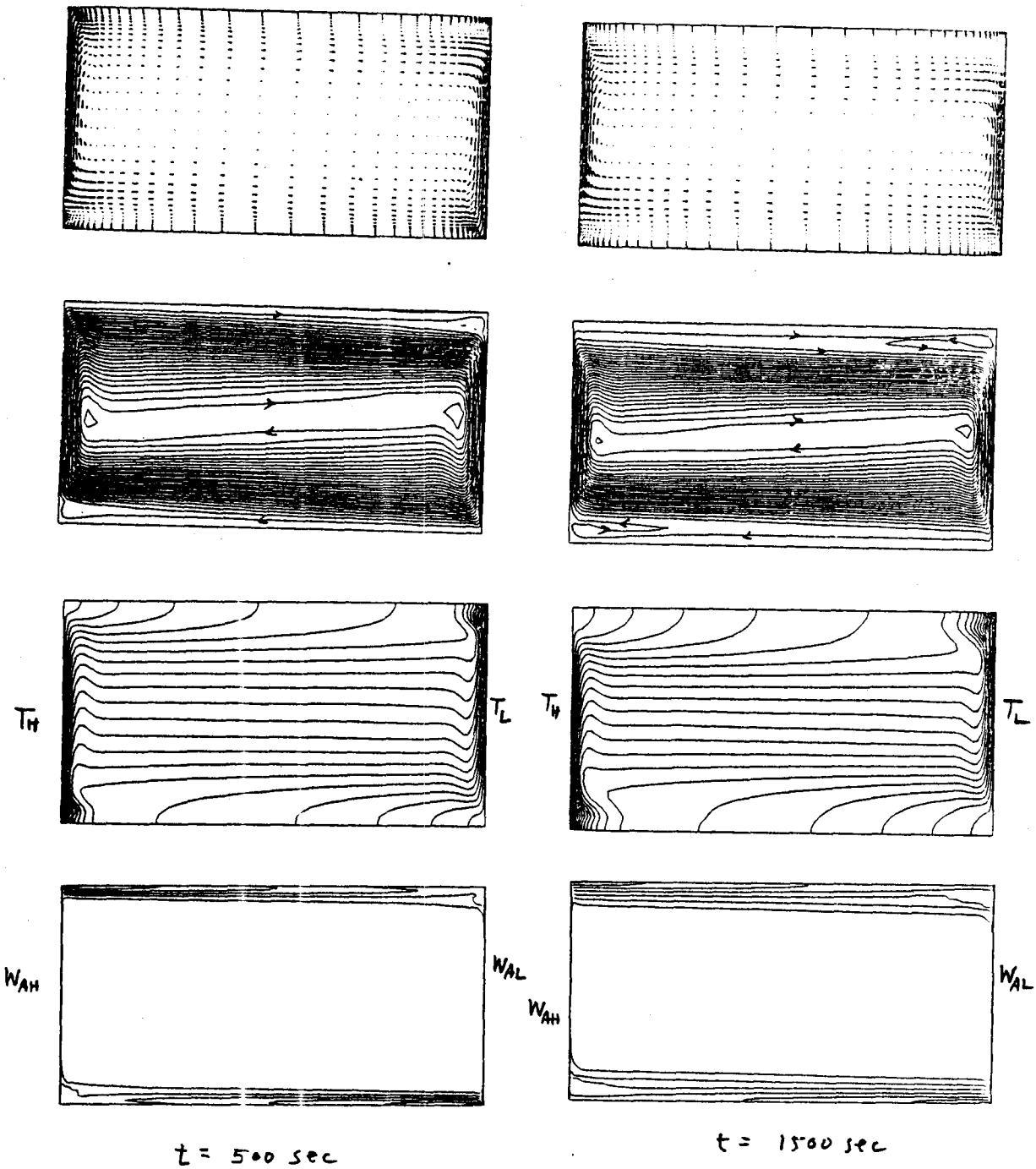

Figure 2. Transient velocity, temperature and solute fields at t=500 sec, t=1500 sec and t=4000sec for case 1 and t=4000sec for case 2.

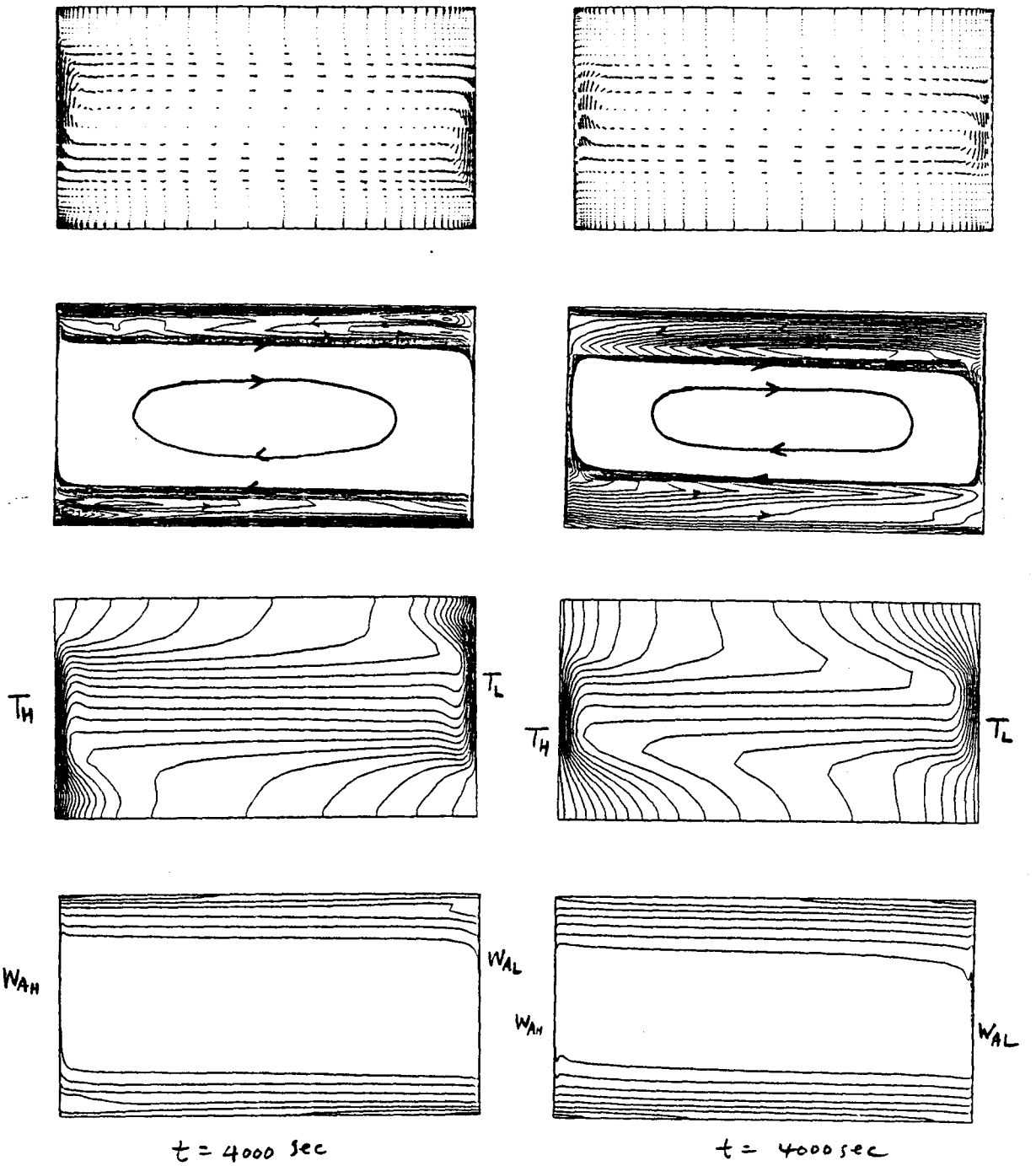

Figure 2. continued (see captions on the previous page)

The most striking feature of the flow field is the appearance of clockwise convection loops near the horizontal surfaces. This feature is in agreement with experimental data reported in ref.[1,7]. The physical explanations offered in ref. [7] are as follows. As species A diffuses from the left wall to the adjacent mixture ,it is carried upward by convection and a thin solute boundary layer develops at the top surface. As the mass transfer continues, the solute boundary layer near the horizontal surface thickens. When the solute boundary layer thickness reaches certain level, some of species A in this solute boundary layer is entrained by the thermally driven convection and swept away from the solute boundary layer. At the right wall, some of this entrained portion of species A can not diffuse to the right wall fast enough to be pulled down by the thermally driven convection at the right wall since mass diffusion is much slower than thermal diffusion. This left over light fluid is then pushed toward the left wall and a clockwise convection loop at the upper right corner of the ampoule appears. Similar double diffusive effects result in a clocwise convection loop at the lower left corner. As time progreses, horizontal solute boundary layer thickness increases (bottom panel) and solute driven weak circulation loops penetrate deeper into the cavity.

Temperature field in the cavity is stronly influenced by the solute transport (third panel). Temperature inversion with a steep gradient is apparent where the solute driven convection loops exist. Therefore, there exist destabilizing temperature gradient and stabilizing solute gradient in these region and flow oscillation of over-stable mode can be triggered [13]. As expected in a high thermal Grashof number convection, the temperature in the core region of the ampoule is completely stratified.

The last column in Figure 2 shows the global flow properties for case 2 at t=4000 sec. The only difference between case 1 and case 2 is that buoyancy force due to the solute transport is in opposite direction. As in the case 1, thermal effects drive the clockwise convection. Due to the solutal effects, weak counter-clockwise convection loops appear near the horizontal walls. These results are not in agreement with observational data [1,7] which show clockwise loops as in case 1.

The solute boundary layer thickness for case 2 is much thicker than case 1 (bottom panel). This may be caused by the increased mixing between the thermal and solute boundary layers at the vertical walls (bottom panel). A strong temperature inversion occurs in the upper right and lower left corner of the ampoule as in case 1.

Comparison with Measurement Data

Figure 3 shows the horizontal velocity (u), nondimensionalized temperature and solute distributions at the

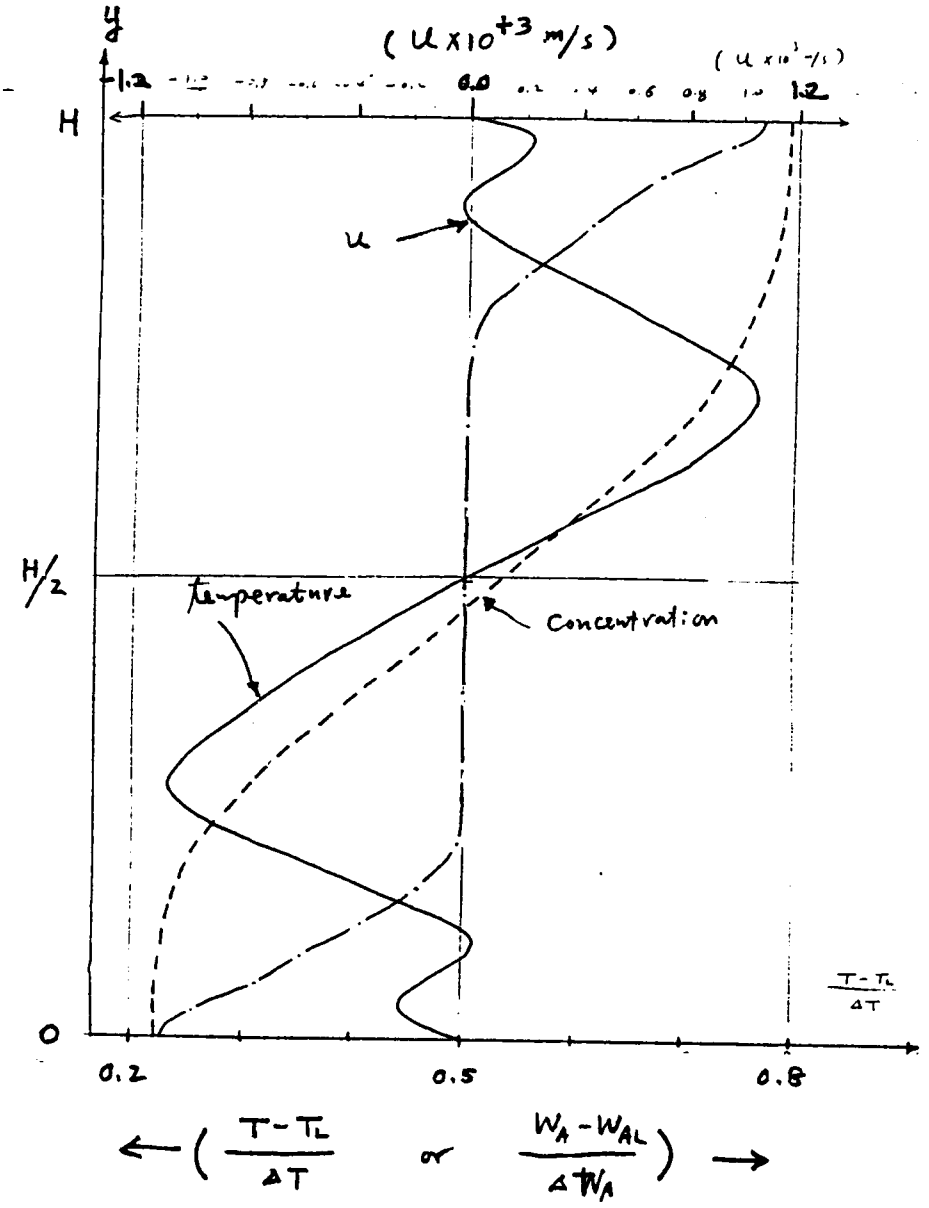

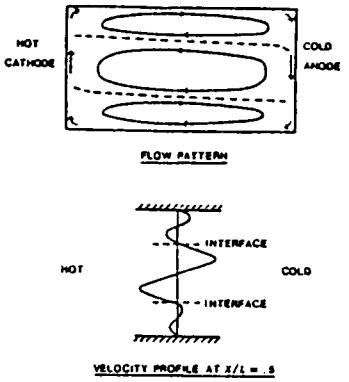

FIG. 2. Layered flow structure for cooperating case.

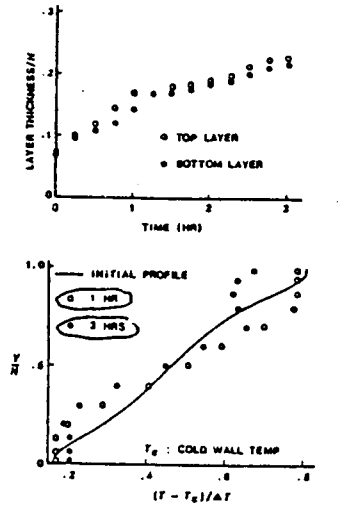

FIG. 4. Changes of layer thicknesses and temperature profile at mid-section for cooperating case with $Ar = 0.55$, $Gr_s = 1.0 \times 10^7$, $Gr_T = 5.4 \times 10^5$ and $N = 18.5$.

Figure 3. Vertical distribution of velocity, temperature and concentration at the center of the cavity for case 1 at t=4000sec. Experimental results taken from refs.[1,7] are shown for comparison.

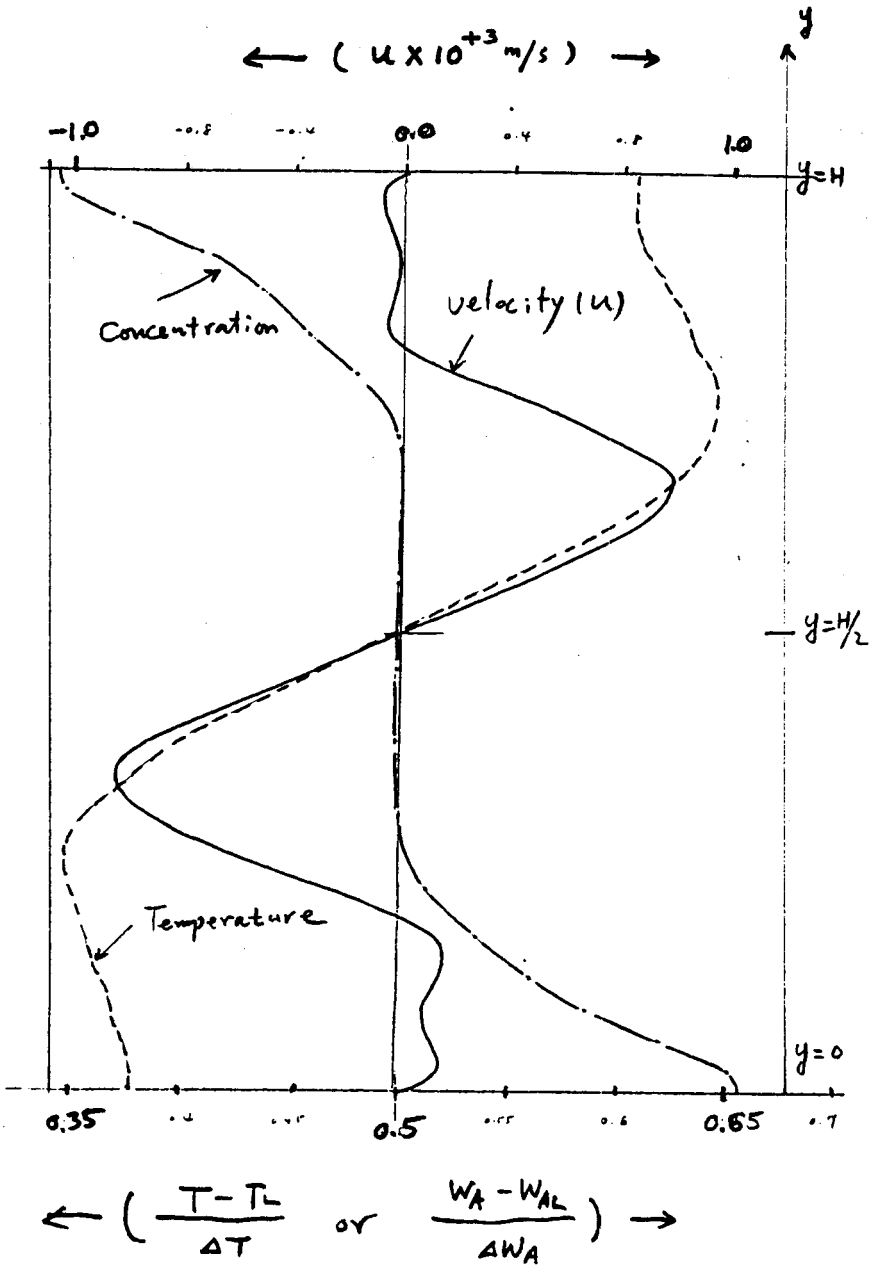

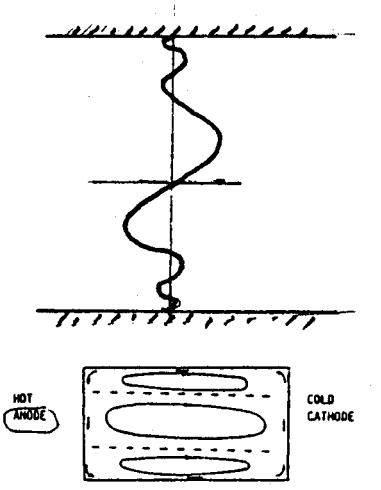

Fig. 16 Sketch of typical flow structure produced at a certain time, showing the layers formed by heating from side for an opposing case
$Gr_T = 6.2 \times 10^5$, $Gr_S = 5.8 \times 10^6$
$A = 0.55$, $Sc = 2.1 \times 10^3$

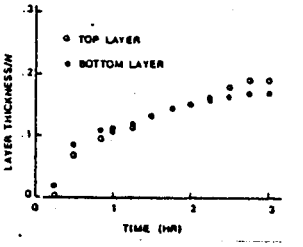

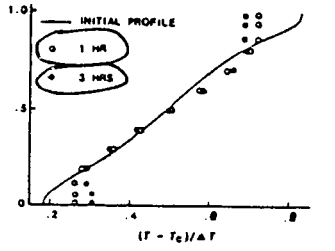

FIG. 7. Changes of layer thicknesses and temperature profile at mid-section for opposing case with $Ar = 0.55$, $Gr_s = 1.0 \times 10^7$, $Gr_T = 6.2 \times 10^5$ and $N = 16.2$.

Figure 4. Vertical distribution of velocity, temperature and concentration at x=L/2 for case 2 at t=4000 sec. Experimental results for a similar case in refs.[1,7] are shown for comparison.

center of the cavity as a function of vertical distance for case 1 at t=4000 sec. Experimental data from ref. [7] are also displayed for comparison. Good qualitative agreements are observed for the velocity and temperature fields. A direct comparison of concentration profiles is not possble since no measurement data is available. The thickness of the solute layer is about 20 % of the cavity height in the present results while it is about 15 % in the measurement.

Figure 4 shows the similar results for case 2 at t=4000 sec. Again experimental data with slightly different conditions [1,7] are shown for comparison. Experimental results show three convective loops rotating clockwise in addition to a thin counter-clockwise circulation due to opposing solutal convection. Numerical results however failed to show two clockwise convection loops near the horizontal surfaces. There exist,however, a crude resemblance between the velocity profiles. Temperature profiles obtained by the numerical simulation show extream inversion while the measument data shows almost uniform temperature in the horizontal solute boundary layer. Solute layer thickness from the present results is about 25 % cavity height while measurement reports only 12 %. Even though some of this discrepancy can be attributed to the difference in the buoyancy ratio used in the present study (18.6) and the measurement (16.2), no satisfactory explanation can be offered.

Average Heat and Mass Transfer

Average heat and mass transfer rate across the cavity are of engineering interest. They are commonly expressed in term of Nusselt number (Nu) and Sherwood number (Sh) defined by

$$Nu = \frac{\text{actual energy transfer by conduction and convection}}{\text{energy transfer by conduction alone}} \qquad (9)$$

and

$$Sh = \frac{\text{actual mass transfer by diffusion and convection}}{\text{mass transfer by diffusion alone}}$$

For a transient heat and mass transfer, Nu and Sh evaluated at the different locations would give different values. They will be constant when a stedy state is reached. Three locations, at the left wall (x=0), at the middle of the cavity (x=L/2) and at the right wall (x=L), are selected to evaluate Nu and Sh in the present study.

Table 3 summarizes the average Nu and Sh numbers evaluated at x=0 at the end of computations. Computations were terminated when the average Sh number variations at x=0 are relatively mild. Even though a true steady-state can not be reached for a very long time because of small mass diffusivity, measurement results [1,7] showed that the mass transfer rate reached a quasi-steady value within a relatively short time. For example, measurement

showed that limiting current (constant mass flux) occurs within 1800 sec for all cases they studied. Numerical results also showed such trend in average Sh numbers . The average Sh numbers in Table 3 represent the quasi-steady values.

Numerical results agree well with the measured Sh for all cases of aiding convection. Discrepancy between two results are within the uncertainty of measurements (10 %). As mentioned in a previous section, horizontal layering of solute near the top and bottom surfaces reduce the cavity height and consequently, thermal convection strength decreases. Therefore, the average Nu number continues to drop as time progresses unlike the average Sh number which reaches a quasi-steady value. Therefore, the average Nu numbers tabulated in Table 3 are not quasi-steady values. Similar trend in reduction of heat transfer by solute layering was also noted in ref.[14].

Table 3. Summary of average heat (Nu) and mass transfer (Sh) rate evaluated at x=0

	present		measurement (ref.7)	
Case	Nu	Sh	Nu	Sh
1	14.95	265.30	-	281.83
2	7.09	215.64	-	-
3	10.32	138.36	-	125.83
4	3.76	119.16	-	-
5	4.14	72.38	-	68.0

From the numerical results, it can be observed that the opposing buoyancy force has much more effects on the heat transfer rate than on the mass transfer rate. In an opposing convection, thermal convection is greatly reduced by the opposing solute buoyancy force and the heat transfer rate becomes smaller. Mass transfer occurs through a thin solute boundary layer at the vertical wall which changes less dramaticlly than the thermal boundary layer.

Figure 5 shows the momentum, thermal and solute boundary layer thickness at x=0, y=H/2. Momentum boundary layer is thicker than the thermal and the thermal boundary is much thicker than the solute boundary layer as expected since Pr=7.07 and Sc=2140.

By reducing the gravity, thermal and solute Gashof numbers are both reduced by the same amount and the average heat and mass transfer rates are equally affected as seen in Table 3. Reducing

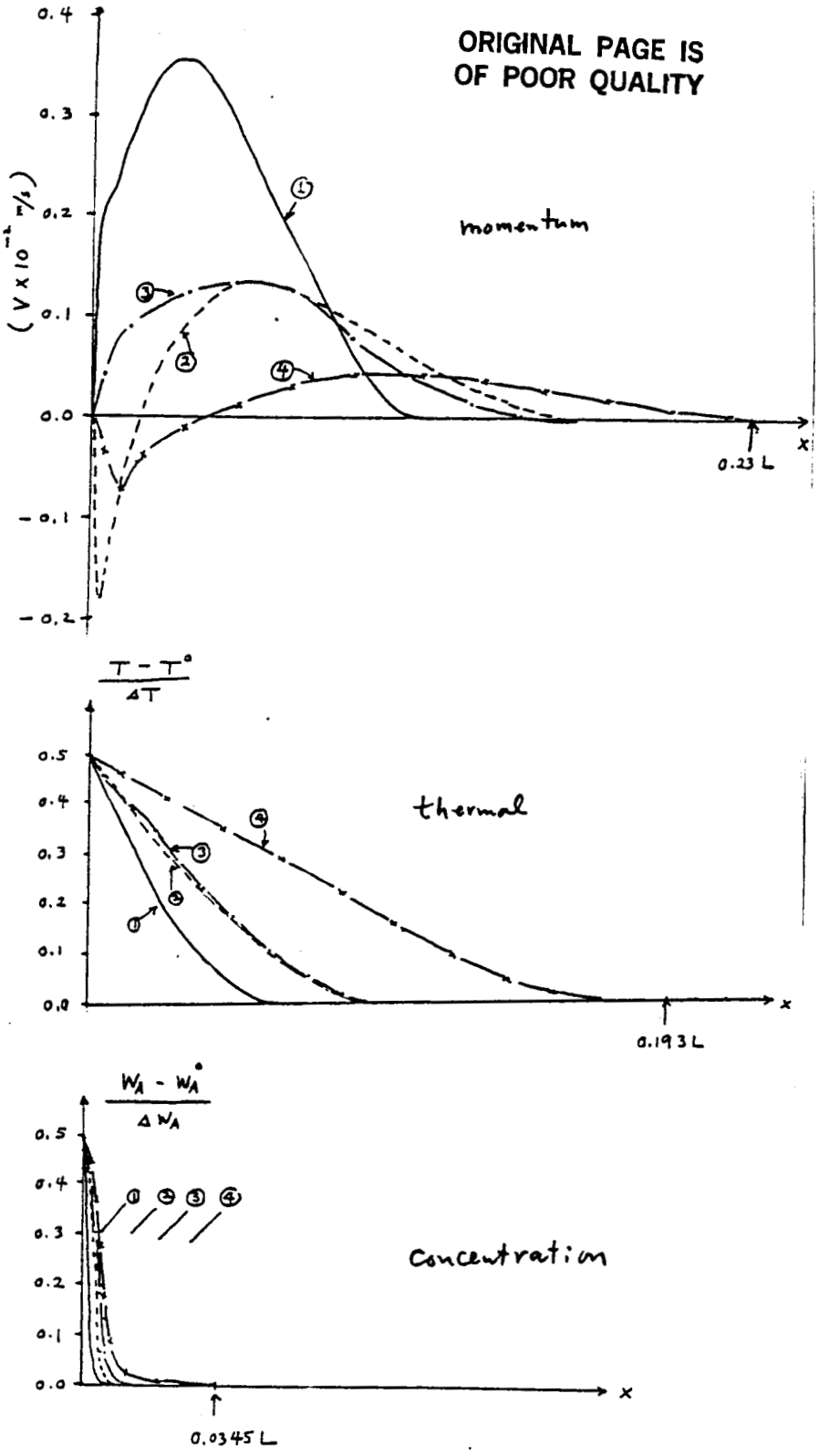

Figure 5. Momentum, thermal and concentration boundary layer thicknesses at the vertical wall at y=H/2 for case 1-4.

the gravity to a level of microgravity environment, say 10e-4g, may not however eliminate the convection effects on the mass transfer. For example, reducing gravity to 0.1g reduces Sh by 48 % (from 265.3 to 138.36) and with 0.01g, 46 % (from 138.36 to 74.0). This shows that the mass transfer is decreased by 50 % by decreasing the gravity ten times. At 1.0e-4g, the average Sh may become 18.75. In order to have Sh=1.0, the gravity may have to be reduced to 1.0e-8g.

Flow Instabilities

Figure 6 shows the transient Nu and Sh number variations for case 2 evaluated at x=0 and x=L/2. Results at x=L are similar to those at x=0 and are not shown. Top panels show the mass transfer rate and the bottom panel shows the heat transfer rate.

Mass transfer evaluated at the wall drops rapidly at the beginning because the mass transfer occurs by diffusion and the solute gradient decreases. The mixture adjacent to the wall begins to move because of solute buoyancy force and the solute boundary layer develops. The concentration at the edge of solute boundary layer is the initial concentration in the ampoule. The mass transfer rate changes very little until convection initiated from the right wall reaches at about t=370 sec. At that time the concentration at the edge of the solute boundary layer begins to drop below the initial concentration and the average mass transfer rate starts to increase.

The mass transfer evaluated at the center remains zero until significant convection of solute occurs at the middle of the ampoule. Note that the mass transfer at the center is carried by convection and diffusion is almost negligible. Mass transfer at the center reaches the maximum when the horizontal velocities near the horizontal walls were the maximum . This occured at about t=370 sec for case 2. Convection strength decreases continually but solute layer near the horizontal walls increases. This is the reason that the average mass transfer rate reaches a quasi-steady value (limiting current value in measurement) rather rapidly. In the present case, this value is reached at about 800 sec.

Mass transfer rate at the wall is seen to increase continuously at t>800 sec. This implies that the solute concentration at the edge of solute boundary layer is being lowered continuously. Mass transfer at the center remains at the quasi-steady value until about 1300 sec at which time oscillation begins. These oscillations peristed until the end of computation while mass transfer rate at the wall remains almost constant. There are two types of oscillations: one with a short oscillation period (about 15 sec) and the other with a relatively long period (about 150 sec).

The behavior of transient heat transfer rate at the wall

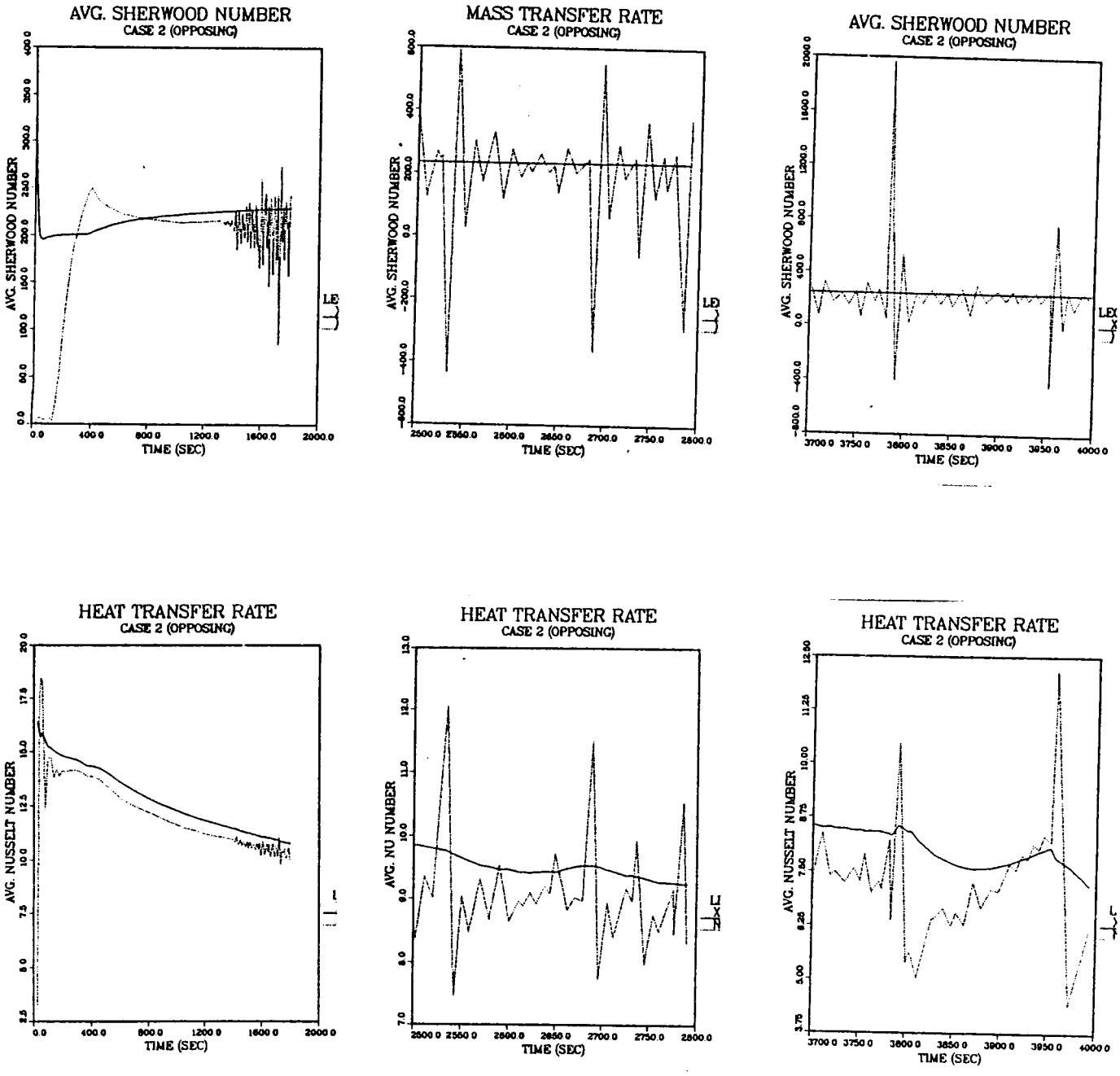

Figure 6. Transient average mass transfer (top panels) and average heat transfer (bottom panels) across the cavity for case 2 evaluated at x=0 (solid lines) and x=L/2 (broken lines).

and at the center can be explained in a similar manner. Since the thermal diffusivity is much larger than the mass diffusiviiity, thermal boudary layer development is much quicker and the thermal boundary layer thickness much larger (see Fig.5). As explained, the heat transfer rate does not reach a quasi-steady value. Instead, they decrease continuously as the effective height of the cavity decreases. Oscillation of Nu follows closely of those of Sh fluctuations.

Some of these oscillations are probably caused by the Brunt-Vaisala instability [15]. Fluid with a destabilizing temperature field (cold fluid on top of warm fluid) is unstable. By using the physical parameters found in the present case, the period of oscillation is found to be

$$\tilde{P} \cong 2\pi \Big/ \left\{ \frac{(\alpha\nu\, Gr_T \cdot Pr)^{1/2}}{\sqrt{1+A^2}} \left(\frac{1}{H^2} \right) \right\} \approx 10.77 \text{ sec} \qquad (10)$$

Other type of short oscillation is caused by the interaction between a destabilizing thermal field and a stabilizing solute field. Using the formula given in ref. [13], the period of oscillation for a over-stable marginal stability for the present case is

$$\tilde{P} \cong 2\pi \Big/ \left[\frac{\mu^2}{3 S_c^2 H^4} \left\{ \frac{Sc(S_c - P_r)}{P_r(P_r+1)} (Gr_s \cdot Pr) - \frac{27\pi^4}{4} \right\} \right]^{1/2} \approx 12.8 \text{ sec} \qquad (11)$$

These two instability mechanisms are probably connected to the short period oscillation observed for Nu and Sh evaluated at the center.

The long period oscillation with large amplitude may be associated with a boundary layer instability at the vertical walls. Interaction among the momentum, energy and thermal buoyancy force are shown to produce such boundary layer instability [16,17]. Since the momentum boundary layer instability produces fluctuations in the velocity boundary layer thickness, thermal boundary thickness will also be affected for moderate Pr number flows. This is indeed the case. Nusselt number at the wall shows such fluctuations. No changes are observed for the Sh at the wall since the solute boundary layer thickness is too small (Sc=2140). Modifying the formula given in ref.[17] for the present case, the period of oscillation is estimated to be

$$\tilde{P} \cong 4\pi^{-1} \nu^{1/3} (g\alpha \Delta T_\delta)^{-2/3} Gr_\delta^{2/3} \approx 150 \text{ sec}, \qquad (12)$$

where ΔT_δ is the temperature difference across the thermal boundary layer and G_{r_δ} is based on the momentum boundary layer thickness.

Similar oscillations of both short and long periods were observed in case 1 as well. Oscillation began at about t=2500 sec in case 1. The critical Grashof number without solutal effects is about 60000 [17]. Grashof number for case 1 and 2 are about 20000. Solute effects, therefore, seem to lower the critical Grashof number over which the velocity boundary layer becomes unstable.

For reduced gavity cases, no boundary layer instabilities were observed. This imples that the critical Grashof number is larger than 2000. The other short periods oscillations were present in reduced gravity cases. But the amplitude of oscillations were very small.

Interfacial Velocity Effects

It is asssumed in the present analysis that the velocity at the vertical walls is zero. In reality, however, horizontal velocity due to diffusion of species A is not zero at these interface between the fluid and the solid. By taking the mass balance at the interface, it can be shown that [18] the horizontal velocity at x=0 and x=L are given by

$$u(x=0,y) = -\frac{D_{AB}}{1-W_A(0,y)} \left.\frac{\partial W_A}{\partial x}\right|_{x=0,y} \qquad (13)$$

and

$$u(x=L,y) = -\frac{D_{AB}}{1-W_A(L,y)} \left.\frac{\partial W_A}{\partial x}\right|_{x=L,y} \qquad (14)$$

respectively.

To show the effects of interfacial velocity, the above velocity conditions were used for case 5 replacing the appropriate boundary conditions. The results showed that the average Sh at x=0 increased by only 2 points. This small change is expected since the interfacial velocity in a dilute solution is very small compared with the characteristic velocity in a moderately large Grashof number convection.

IV. CONCLUSIONS AND RECOMMENDATIONS

In conclusions, a two-dimensional time-dependent numerical analysis are used to investigate the thermal and solute interactions encountered in a solution growth of single crystals. Numerical results were compared with experimental data. Good quantitative agreements were obtained in term of average mass transfer rate. Good qualitative agreements of over-all convection fields were also observed.

It was observed that the thermal and solute fields become highly oscillatory when the Grashof number are large. Oscillations are probably cauesd by a number of instability mechanisms. Some of these instabilities were seen to disappear at the reduced gravity environments.

Transient temperature and solute distributions are found to be fairly non-uniform at the cryatal growing surface (x=L). And the effects of convection on the solute transport may not be negligible even in the micro-gravity environment with 1.0e-4g.

The following is recommended for the extension of the present study:

1. It is further needed to veryfy the capability of the numerical method used in the present study by simulating other experimental data. (Lack of satisfactory agreement between the numerical and experimental results for case 2 should be adequately explained.) One possible source of disagreement is the numerical diffusion. A higher order numerical approximation may be needed.

2. Analyse other solution growth situations with realistic physical and flow parameters, such as mixture properties, ampoule geometries and bondary conditons (including segregation effects) .

3. Perform a fundamental numerical study on the instability mechanisms encountered over simple geometries such as vertical and horizontal planes.

4. Extend to three-dimensional cases if success is warranted.

REFERENCES

1. Ostrach, Simon, "Fluid Mechanics in Crystal Growth , 1982 Freeman Scholar Lecture," J. Fluid Eng., Vol. 105, 5-20, 1982.

2. Rosenberger, F., Fundamentals of Crystal Growth, Vol. 1, Macroscopic Equilibrium and Transport Concepts, p. 360, Springer, Berlin, 1979.

3. Pimputkar, S. M.,and Ostrach, S.,"Convective Effects in Crystal Grown from Melt," J.Crystal Growth, 55, p.614, 1981.

4. Chang, C. J., and Brown, R. A.,"Radial Segregation Induced by Natural Convection and Melt/Solid Interface Shape in Vertical Bridgeman Growth,' J. Crystal Growth, 63, p.343, 1983.

5. Murthy, J. Y., "A Numerical Simulation of Flow, Heat and Mass Transfer in A Floating Zone At High Rotational Reynolds Numbers," J. Crystal Growth, 83, p.23, 1987.

6. Extremet, G., Roux, B., Bontoux, P., and Elie, F., "Two-dimensional Model for Thermal and Solutal Convection in Multizone Physical Vapor Transport," J. Crystal Growth, 82, p.761, 1987.

7. Kamotani, Y., Wang, L. W., Ostrach, S., and Jiang H. D., "Experimental Study of Natural Convection in Shallow Enclosure with Horizontal Temperature and Concentration Gradients," Int. J. Heat, Mass Transfer, 28, p.165, 1985.

8. Patankar, S. V.,Numerical Heat Transfer and Fluid Flow, McGraw-Hill, 1980.

9. Han, S. M., "A Generalized Implicit Finite Difference Method for Transient Analysis of Compressible and Incompressible Fluid Flow," in Numerical Methods for Fluid Transient Analysis, ASME FED-Vol.4, Martin and Chaudry(editors),p.17, 1983.

10. Van Doormal, J. P., and Raithby, G. D.,"Enhancement of the SIMPLE Method for Predicting Incompressible Fluid Flows," Numerical Heat Transfer, Vol.7, p.147, 1984.

11. Han, S. S., and Schafer, C. F., "Transient Natural Convection Heat and Mass Transfer in A Rectaangular Enclosure: A Numerical Analysis," in Development of Theoretical and Applied Mechanics, Vol. 14, Hackett and Wang (editors), 1988.

12. Turner, J. S.,"Double-Diffusive Phenomena," Ann. Rev. Fluid Mech., Vol. 6, p.37, 1974.

13. Shirtcliffe, T. G. L., "An Experimental Investigation of Thermosolutal Convection at Marginal Stability," J. Fluid Mech., Vol.35, p.677, 1969.

14. Writz, R. A.,"The Effect of Solute Layering on Lateral Heat Transfer in an Enclosure," Int. J. Heat,Mass Transfer, Vol.20, p.841, 1977.

15. Patterson, J., and Imberger, J.,"Unsteady Natural Convection in a Rectangular Cavity," J. Fluid Mech., Vol.100, p.65, 1980.

16. Gebhart, B. "Instability, Transition, and Turbulence in Buoyancy-Induced Flows'" Ann. Rev. Fluid Mech., Vol.5, p.213, 1973.

17. Carruthers, J. R,"Origin of Convective Temperature Oscillations in Crystal Growth Melts," J. Crystal Growth, 32, p.13, 1976.

18. Greenwell, D. W., Markham, B. L., and Rosenberger, F., "Numerical Modeling og Diffusive Physical Vapor Transport in Cylindrical Ampoules," J. Crystal Growth, 51, p.413, 1981.